Genetic Architecture of Heart Mitochondrial Proteome influencing Cardiac Hypertrophy

Short title: Mitochondria and Heart Failure

Karthickeyan Chella Krishnan[1*], Elie-Julien El Hachem[2], Luke Carroll[3], Alexis Diaz Vegas[3], Christine Light[4], Yang Cao[5], Calvin Pan[5], Karolina Elżbieta Kaczor-Urbanowicz[6,7], Varun Shravah[8], Diana Anum[9], Matteo Pellegrini[7], Chi Fung Lee[4,10], Marcus M. Seldin[11,12], Benjamin L. Parker[13], David E. James[3] and Aldons J. Lusis[6,14,15*]

[1]Department of Pharmacology and Systems Physiology, University of Cincinnati College of Medicine, OH, USA

[2]Department of Integrative Biology and Physiology, Field Systems Biology, Sciences Sorbonne Université, Paris, France

[3]Metabolic Systems Biology Laboratory, Charles Perkins Centre, School of Life and Environmental Sciences, University of Sydney, Sydney, New South Wales, Australia

[4]Cardiovascular Biology Research Program, Oklahoma Medical Research Foundation, Oklahoma City, OK, USA

[5]Department of Medicine/Division of Cardiology, [6]Division of Oral Biology and Medicine, UCLA School of Dentistry, [7]UCLA Institute for Quantitative and Computational Biosciences, [8]Department of Chemistry and [9]Department of Integrative Biology and Physiology, University of California, Los Angeles, CA, USA

[10]Department of Physiology, University of Oklahoma Health Sciences Center, Oklahoma City, OK, USA

[11]Center for Epigenetics and Metabolism and [12]Department of Biological Chemistry, University of California Irvine, CA, USA

[13]Department of Anatomy and Physiology, University of Melbourne, Melbourne, Victoria, Australia

[14]Department of Human Genetics and [15]Department of Microbiology, Immunology and Molecular Genetics, University of California, Los Angeles, CA, USA

[*]Correspondence: chellakn@ucmail.uc.edu (K.C.K) and jlusis@mednet.ucla.edu (A.J.L)

ABSTRACT

Mitochondria play a key role in the normal function of the heart as well as in the pathogenesis of diseases. We report analysis of common genetic variations contributing to mitochondrial and heart functions using an integrative proteomics approach in a panel of inbred mouse strains called the Hybrid Mouse Diversity Panel (HMDP). We performed a whole heart proteomic analysis in the HMDP (72 strains, n=2-3 mice) and retrieved 840 mitochondrial proteins (quantified in ≥50 strains). High-resolution association mapping on their respective abundance levels identified three *trans*-acting genetic loci, located on chromosome (chr) 7, chr13 and chr17, that control distinct classes of mitochondrial proteins as well as heart hypertrophy. Follow-up high resolution regional mapping identified NDUFS4, LRPPRC and COQ7 as the candidate genes for chr13, chr17 and chr7 loci, respectively, and both experimental and statistical analyses supported their causal roles. Variations of all three were associated with heart mass in two independent heart stress models, namely, isoproterenol (ISO)-induced heart failure and diet-induced obesity (DIO) models. To identify the aspects of mitochondrial metabolism regulated by these loci, we constructed co-expression protein networks using weighted gene co-expression network analysis (WGCNA). DAVID enrichment analyses of genes regulated by each of the loci revealed that the chr13 locus was highly enriched for complex-I proteins (24 proteins, P = 2.2E-61), the chr17 locus for mitochondrial ribonucleoprotein complex (17 proteins, P = 3.1E-25) and the chr7 locus for ubiquinone biosynthesis (3 proteins, P = 6.9E-05). These results indicate that common variations of certain mitochondrial proteins can act in *trans* to influence mitochondrial functions and contribute to heart hypertrophy, elucidating mechanisms that may underlie genetic susceptibility to heart failure in human populations.

KEYWORDS

Natural genetic variation; Systems genetics; Mitochondria; Heart Failure.

SUBJECT CODES

Proteomics; Metabolic Syndrome; Genetic, Association Studies; Hypertrophy; Heart Failure.

NONSTANDARD ABBREVIATIONS AND ACRONYMS

HMDP	hybrid mouse diversity panel
WGCNA	weighted gene co-expression network analysis
pQTL/s	protein quantitative trait locus/loci
ISO	isoproterenol
DIO	diet-induced obesity
miR	microRNA
NDUFS4	NADH-ubiquinone oxidoreductase subunit S4 or NADH dehydrogenase [ubiquinone] iron-sulfur protein 4, mitochondrial
NRVM	neonatal rat ventricular myocytes
LRPPRC	leucine-rich pentatricopeptide repeat motif-containing protein
SLIRP	SRA stem-loop interacting RNA binding protein
COQ7	coenzyme Q7, hydroxylase or mitochondrial 5-demethoxyubiquinone hydroxylase
CoQ	coenzyme Q or ubiquinone

INTRODUCTION

Mitochondrial functions play a major role in the pathophysiology of several metabolic syndrome traits including obesity, insulin resistance and fatty liver disease (1-5). There is now substantial evidence showing that genetic variation in mitochondrial functions contribute importantly to 'complex' diseases such as cardiovascular diseases (CVD) (6). A scientific statement from the American Heart Association summarizes the central role of mitochondria in heart disease (7). Mitochondrial bioenergetics and other functions impinge on virtually all aspects of the cell, including energy, cellular redox, apoptosis, and substrates for epigenetic modifications. Mitochondrial dysfunction also contributes to the development of heart failure (8, 9). The primary putative mechanism linking mitochondrial dysfunction to heart failure is decreased oxidative respiration leading to contractile failure. However, many other mechanisms have been postulated in recent years to implicate mitochondrial dysfunction in heart failure. They include excessive oxidative stress leading to inflammation, cell damage, and cell death; disturbed calcium homeostasis that triggers the opening of the mitochondrial permeability transition pore (mPTP), leading to loss of membrane potential, and eventual cell death. Therefore, mitochondria are an attractive target for heart failure therapy (8). Despite evidence showing that genetic variation in mitochondrial proteins are linked to disease, most studies tend to overlook the role of genetic variation in exploring the link between mitochondrial function and relevant phenotypes. To this end, we employ a 'systems genetics' approach to address this issue.

Our laboratory uses a combination of genetics, molecular biology, and informatics to investigate pathways underlying common cardiovascular and metabolic disorders. We exploit natural genetic variation among inbred strains of mice (and among human populations where possible) to identify novel targets and formulate hypotheses, taking advantage of unbiased global multi-omics technologies, such as transcriptomics, metabolomics, and proteomics, to help decipher causal mechanisms that drive complex traits. This 'systems genetics' approach integrates natural genetic variation with omics-level data (such as global protein abundance levels) to examine complex interactions that are difficult to address directly in humans. It shares with systems biology a holistic, global perspective (10, 11). Typically, a genetic reference population is examined for relevant clinical traits as well as global molecular traits, such as

proteomics, and the data are integrated using correlation structure, genetic mapping, and mathematical modeling (10, 11).

Our systems genetics approach utilizes a well-characterized genetic reference population of 100 inbred mice strains, termed the Hybrid Mouse Diversity Panel (HMDP) (12). The design of the HMDP resource, consisting of a panel of permanent inbred strains of mice that can be examined for many phenotypes, has proved invaluable for studying metabolic syndrome traits. Major advantages of this approach are that the mapping resolution for complex traits is superior to traditional genetic crosses and the use of inbred strains affords replication of biological measures. It also facilitates studies of gene-by-environment and gene-by-sex interactions, which are difficult to address in human populations. Using this resource, we have characterized several cardiometabolic traits in both sexes over the last 10 years (13-27).

In the present study, we have explored the genetic regulation of mitochondrial pathways and their contribution to heart function in the HMDP. Using an integrative proteomics approach, we now report the identification of three independent genetic loci that control distinct classes of mitochondrial proteins as well as heart hypertrophy. Each locus contains proteins previously shown to affect heart pathophysiology but by unknown mechanisms. Our results show that genetic diversity in the mitochondrial proteome plays a central role in heart pathophysiology.

RESULTS

Genetic architecture of the heart mitochondrial proteome revealed three *trans*-regulatory hotspots.

To investigate the effects of genetics on the heart proteome, we first performed a whole heart proteomic analysis in the HMDP (72 strains, n=2-3 mice, female sex; listed in Table S1) and surveyed mitochondrial localization using MitoCarta2.0 (28). We retrieved abundance data for 840 of these proteins (quantified in ≥50 strains) and performed high-resolution association mapping on their respective abundance levels to the HMDP genotypes. Genetic variants associated to the protein abundance of nearby genes (<1Mb) were referred to as *cis*- protein quantitative trait loci (pQTLs) and the remainder were referred to as *trans*-pQTLs. When a *trans*-pQTL locus is associated to multiple proteins, we defined it as a *trans*-pQTL hotspot. Using

these criteria, we identified three hotspots, located on chromosome (chr) 7, chr13 and chr17, respectively (Figure 1A).

To identify the aspects of mitochondrial metabolism regulated by these loci, we constructed co-expression protein networks using weighted gene co-expression network analysis (WGCNA) (29) and identified five modules (Figure 1B). Eigengenes, representing the first principal component of two of these modules (Brown and Green), mapped to the same regions as the chr13 and chr17 loci, respectively. DAVID enrichment analyses (30) revealed that the chr13 locus (26 proteins; Figure 2A and Table S2) that overlapped with Brown module (72 proteins, 96% overlap) was highly enriched for mitochondrial complex-I proteins (24 proteins, P = 2.2E-61), and the chr17 locus (22 proteins; Figure 3A and Table S3) that overlapped with Green module (44 proteins, 73% overlap) was highly enriched for mitochondrial ribonucleoprotein complex proteins (17 proteins, P = 3.1E-25). The hotspot proteins in the chr7 locus (27 proteins; Figure 4A and Table S4) were found primarily in the Turquoise module (393 proteins, 81% overlap) and was highly enriched for ubiquinone biosynthesis (3 proteins, P = 6.9E-05).

Chr13 locus controls mitochondrial complex-I.

First, we analyzed the chr13 locus (26 proteins) that was highly enriched for mitochondrial complex-I (Figure 2A). Mapping the eigengene of the chr13 *trans*-regulated proteins identified the peak SNP (rs48592660). NDUFS4, a protein critical for complex-I assembly and loss of which leads to cardiac hypertrophy (2) mapped near the locus but outside the region of linkage disequilibrium. However, within the locus was the *microRNA(miR)-23b/27b/24-1* cluster, among which *miR-27b*, a conserved regulator of NDUFS4, was identified *via* nine miRNA target prediction algorithms and one dataset of experimentally validated miRNA targets (Figure 2B and Table S5). Cardiac overexpression of *miR-27b* has previously been shown to promote cardiac hypertrophy (31) but attenuate angiotensin II-induced atrial fibrosis (32). We therefore hypothesized that the chr13 locus regulated complex-I proteins by influencing *miR-27b* and thus NDUFS4 protein levels. Indeed, we observed higher levels of both the chr13 locus eigengene and NDUFS4 with the GG allele of the peak locus SNP (Figure 2C). To identify the functional relevance of this peak SNP, we analyzed its association in two independent heart stress models, namely, isoproterenol (ISO)-induced heart failure (17) and diet-induced obesity (DIO) (13)

models. We observed significantly lower left ventricular mass under ISO stress (Figures 2D) and lower heart weight under DIO stress in both sexes (Figures 2E) of strains harboring the GG allele, thus confirming the directionality of genetic impacts on NDUFS4 protein levels and hypertrophic response.

NDUFS4 heart-specific knockout mice had reduced mitochondrial complex-I proteins. NDUFS4 is an 18-kDa accessory subunit that is essential for the mitochondrial complex-I assembly (33-37). Loss of function mutations in NDUFS4 leads to complex-I deficiency causing a neuromuscular disease, Leigh syndrome (38) and is also involved in cardiomyopathies (2, 39, 40). Taken together, we wanted to experimentally test our hypothesis that NDUFS4 protein independently controls the complex-I protein abundance levels in heart. For this, we performed whole heart proteomic analyses in both control and heart-specific *Ndufs4*-cKO mice (n = 5 mice/group). Among the abundance data for 3575 proteins, we observed 31 proteins to be significantly different between the control and cKO groups (significance cutoff: abs[$\log_2$FC] > 1 and $P_{adj} < 0.001$; listed in Table S6). Strikingly, 21 of these proteins were found in the chr13 locus and these were highly enriched for complex-I proteins (30 proteins, P = 3.8E-80). Notably, only one protein, NDUFAF2, was up regulated in *Ndufs4*-cKO mice (Figure 2G). This is intriguing because NDUFAF2 has been reported to stabilize complex-I in the absence of NDUFS4 and to sustain complex-I activity (41, 42) indicating this may be a compensatory mechanism.

***MiR-27b* controls NDUFS4 protein levels and heart weights.** As an independent corroboration and to understand the consequence of the chr13 locus on *miR-27b* expression, we independently sequenced miRNAs from DIO-stressed female HMDP strains (n = 85 strains). We found that strains harboring the GG allele had significantly higher *miR-27b* expression (Figure 2H), and there was a significant inverse correlation between heart weights and *miR-27b* expression in these mice (Figure 2I). Based on these observations, we hypothesize that *miR-27b* increases NDUFS4 protein levels thereby reducing heart weights. To validate this observation, we transfected neonatal rat ventricular myocytes (NRVMs) with mature *miR-27b* in the presence or absence of phenylephrine (PE) treatment. Immunoblot analyses revealed that NDUFS4 protein levels were reduced with PE treatment in the control cells but *miR-27b-3p*

consistently increased NDUFS4 protein levels in both control and PE-treated conditions (Figure 2J). Taken together, we conclude that the chr13 locus affects mitochondrial complex-I proteins through the *miR-27b*/NDUFS4 axis, thereby controlling heart weights.

Chr17 locus controls mitoribosomes.

Next, we analyzed the chr17 locus (22 proteins) that was highly enriched for mitochondrial ribosomal proteins (Figure 3A). We mapped the eigengene of the significantly associated mitochondrial proteins to identify the peak SNP (rs46340181). We identified LRPPRC as a candidate as it was the only protein controlled in *cis* by the peak SNP (Figure 3B). Importantly, LRPPRC together with SLIRP controls mitochondrial mRNA stability, enabling polyadenylation and translation (43-45). Loss of function mutations in LRPPRC cause a congenital mitochondrial disease called Leigh syndrome, French-Canadian type that is often characterized by mitochondrial complex IV deficiency and impaired mitochondrial respiration (46, 47). It is noteworthy that SLIRP is also under the control of the chr17 locus (Figure 3A). Further, our phenotypic associations revealed that the eigengene and LRPPRC were inversely associated with the TT allele (Figure 3C). This was functionally translated into lower heart weight in strains harboring the TT allele in both sexes under DIO stress only (Figures 3D – 3F). We also observed that abundance levels of both LRPPRC and SLIRP proteins were strongly correlated with each other (Figure 3G) and controlled by the chr17 locus (Figure 3A), thus demonstrating that they are co-regulated.

LRPPRC/SLIRP protein complex controls mitochondrial transcript levels.

Based on our current observations and published data, we hypothesized that high LRPPRC/SLIRP protein complex stabilizes mitochondrial transcripts, thus reducing the need to upregulate mitochondrial translation. To test this, we independently sequenced the heart transcripts from our HMDP mice that underwent DIO stress. We observed that the chr17 locus peak SNP (rs46340181), which strongly controls both LRPPRC and SLIRP proteins, is only associated with the mitochondrial mRNA expression and not their respective protein levels (Figure 3H). Moreover, this phenomenon was observed in both sexes, explaining the lack of sex bias in phenotypic associations (Figures 3E – 3F). In contrast, the chr13 locus that controlled complex-I proteins did not show strong associations with transcript levels in either sex (Figure 3I

– 3J). As a specific example, Figure 3I shows that the mRNA expression of *mt-ND1* was higher in strains harboring the TT allele in both sexes under DIO stress, illustrating that upregulated LRPPRC/SLIRP is stabilizing the mitochondrial transcript (Figure 3C), resulting in reduced heart weights (Figures 3D – 3F).

Chr7 locus affects CoQ metabolism.

Finally, we analyzed the chr7 locus (27 proteins), which unlike the chr13 or chr17 loci, had no major representation of a single mitochondrial protein complex but was moderately enriched for ubiquinone biosynthesis (Figure 4A). Mapping the eigengene of the significantly associated mitochondrial proteins identified the peak SNP (rs32451909). We identified COQ7 as a strong candidate as it was the only protein exhibiting a *cis*-regulation at the locus in the region of linkage disequilibrium (Figure 4B). COQ7 catalyzes a critical step in the biosynthesis of coenzyme Q (CoQ). Among several functions, CoQ participates in electron transport facilitating ATP synthesis. CoQ also has a clear role in heart failure (48). Phenotypically, we observed lower levels of both the eigengene and COQ7 with the GG allele (Figure 4C). This was functionally translated into higher heart weight in strains containing GG allele in both sexes under DIO stress only (Figures 4D – 4F). We also observed that abundance levels of other COQ proteins were strongly correlated with COQ7 protein, thus demonstrating that they are co-regulated (Figures 4G – 4I). At least two of these proteins, COQ3 and COQ6, are controlled by the chr7 locus (Figure 4A). When we measured the CoQ levels in both the mitochondrial fractions and total heart lysates from DIO-stressed female HMDP strains (n = 15 strains), we observed a significant upregulation in the levels of both CoQ9 and CoQ10 only in the lysates from HMDP mice harboring the GG allele (Figure 4J). Taken together, we conclude that the chr7 locus controls CoQ metabolism *via* regulation of the COQ7 protein.

DISCUSSION

We have previously used systems genetics analyses in HMDP and discovered a central role for adipose mitochondrial function in the sex differences observed in cardiometabolic traits, including obesity, insulin resistance and plasma lipids (26, 27), and liver mitochondrial function in non-alcoholic fatty liver disease (24). In the present study, an integrative proteomics approach was utilized in HMDP to investigate the effects of genetic regulation of mitochondrial pathways

on heart function. Several conclusions have emerged. First, we identified three distinct and independent *trans*-regulating genetic loci, on chr13, chr17 and chr7, respectively. Second, our enrichment analyses have suggested mechanisms perturbed by each of these loci. Thus, the chr13 locus was enriched for mitochondrial complex I, chr17 for mitoribosomes, and chr7 was enriched for ubiquinone biosynthesis. Third, our regional mapping identified NDUFS4, LRPPRC and COQ7 as the candidate genes for chr13, chr17 and chr7 loci, respectively. Finally, we performed both experimental and statistical analyses to support their causal roles. Each of these points is discussed in detail below.

Trans-acting human pQTLs, mostly using blood/plasma proteome (49-54), and *trans*-acting human eQTLs (55-59), have been reported, but exploring *trans*-regulatory landscapes in human studies is limited by sample size, tissue accessibility, and environmental factors. In the current study, mapping genetic loci controlling protein abundance levels in heart tissues from an inbred mouse population revealed that ~9% of available nuclear-encoded mitochondrial proteins (75/840) are significantly controlled ($P < 1E-6$) by three genetic loci, on chr13 (26 proteins), chr17 (22 proteins) and chr7 (27 proteins), respectively. Each of these three *trans* regulating hotspots were specific for the proteome, as they were not identified in our heart transcriptome. Interestingly, two of these hotspots independently controlled mitochondrial complex I, one at the mRNA (chr17 *via* LRPPRC/SLIRP) and the other at the protein level (chr13 *via miR-27b*/NDUFS4). Finally, the chr7 locus was found to control ubiquinone metabolism *via* COQ7 protein.

Mitochondrial complex I is the first and largest (~1-MDa) protein complex of the mitochondrial electron transport chain comprised of 45 subunits, seven encoded in the mtDNA (33, 60, 61). NDUFS4 is an 18-kDa accessory subunit that assembles the catalytic N-module (where NADH oxidation occurs) with the rest of the complex I. Mutations leading to the loss of NDUFS4 result in complex I deficiency (33-37) and are involved in cardiomyopathies, both in protective (ischemia/reperfusion injury) and detrimental roles (pressure overload) (2, 39, 40). It was also reported that loss of NDUFS4 causes reduced complex I mediated ROS generation (ischemia/reperfusion injury) and increased protein acetylation (pressure overload), leading to their respective pathologies. Here we demonstrate that heart specific NDUFS4 KO mice have

higher levels of NDUFAF2, which is reported to partly stabilize complex I in the absence of NDUFS4, although the resultant complex I is unstable and has reduced activity (41). Taken together, we report that natural variation in NDUFS4 protein levels affect other complex I proteins resulting in reduced complex I activity and cardiac hypertrophy. On the other hand, the role of *miR-27b* on heart function is unclear. Cardiac-specific overexpression of *miR-27b* has been reported to increase pressure overload-induced cardiac hypertrophy *via* PPARG (31) but attenuated angiotensin II-induced atrial fibrosis *via* ALK5 (32). Also, whole body knockout of *miR-27b* was found to attenuate pressure overload-induced cardiac hypertrophy *via* FGF1 (62), but this could be due to extracardiac effects mediated by *miR-27b-3p* such as adipocyte browning (63-65). Using 100 inbred strains of mice, here we report that cardiac *miR-27b* expression was inversely correlated with heart weights and that mature *miR-27b-3p* appears to have a protective role in reducing cardiac hypertrophy *via* increasing NDUFS4 protein levels.

Mitochondria are unique organelles having their own genome that encodes for 13 protein coding genes, which are essential subunits of complexes I, III, IV and V. Nuclear-encoded LRPPRC protein working together with the SLIRP protein helps to enable mitochondrial mRNA translation *via* promoting its polyadenylation and stability (43-45). Loss of function mutations in LRPPRC causes Leigh syndrome, French-Canadian type that are associated with complex IV deficiency and impaired mitochondrial respiration (46, 47). Here we show that natural genetic variations in a panel of inbred mouse strains at a chr17 locus (TT allele) result in higher protein levels of the LRPPRC/SLIRP complex as well as lower heart weights. This phenomenon is most likely mediated by increased expression levels of mitochondrial mRNA that coincide with reduced protein levels of mitoribosomes. We propose that since these mitochondrial mRNAs are protected by LRPPRC/SLIRP complex, fewer mitoribosomes are necessary for translation. Interestingly, though LRPPRC mutations are often associated with complex IV deficiency (46, 47), we observed that complex I mRNAs were also strongly regulated by the LRPPRC/SLIRP complex, in addition to complex IV mRNAs. Thus, further research on the bioenergetic consequences of LRPPRC/SLIRP loss of function mutations beyond complex IV deficiency are warranted.

Mitochondrial coenzyme Q, or ubiquinone or CoQ, is essential for mitochondrial electron transport chain function as it shuttles electrons from both complexes I and II to complex III. The enzyme COQ7 is responsible for catalyzing the penultimate step in CoQ biosynthesis. Here we report that the chr7 locus (GG allele) is associated with reduced levels of COQ7 protein, which is in turn associated with increased heart weights. Interestingly, when we measured CoQ levels in these hearts, we found no differences in the mitochondrial fractions but an increase in both CoQ9 and CoQ10 levels in the lysates. Mice with a complete loss of *Coq7* expression have embryonic lethality (66) but survive for several months after a knockout is induced in the adult (67). Interestingly, *Coq7* heterozygous knockout mice are long-lived but exhibit dysfunctional mitochondria (such as reduced respiration, reduced ATP levels and increased ROS generation) with no differences in CoQ levels despite significantly reduced COQ7 protein levels (68-70). Furthermore, these *Coq7* heterozygous knockout mice were found to harbor a varying distribution of CoQ9 levels in their liver mitochondria with the outer membrane having increased CoQ9 while the inner membrane had reduced CoQ9 levels (71). It was postulated that higher CoQ9 levels in the liver mitochondrial outer membrane may be a protective response to increased ROS levels generated in *Coq7* heterozygous knockout mice (71). Thus, reduced COQ7 protein levels do not necessarily associate with reduced CoQ levels but have heterogeneous sub-mitochondrial and possibly subcellular CoQ distributions. Taken together, we propose that increased heart weights in mice harboring chr7 locus (GG allele) is a result of increased ROS generation caused by reduced COQ7 protein levels. Also, the increased CoQ levels in the heart lysates of these mice might be a protective response against the oxidative stress generated by reduced COQ7 protein in these mice. Further research is warranted in understanding the purported role of COQ7 in submitochondrial and subcellular CoQ heterogeneous distribution focusing on heart pathophysiology.

In conclusion, our unbiased systems genetics analyses identified three loci regulating mitochondrial function in the heart. None of these loci were observed when transcript levels were examined, providing justification for proteomic rather than transcriptomic studies. All three loci are associated with heart mass in two independent heart stress models. The results provide mechanistic information about the roles of previously studied genes namely, NDUFS4, LRPPRC and COQ7, in heart failure.

METHODS

Mice

All mice were purchased from The Jackson Laboratory and bred at UCLA according to approved institutional animal care and use committee (IACUC) protocols with daily monitoring. Both the ISO-induced HF (15, 17, 19) and DIO (13, 14) models were previously described in detail. Briefly, for ISO-induced HF model, 8 to10 weeks of age female mice were administered with isoproterenol (30 mg per kg body weight per day, Sigma) for 21 days using ALZET osmotic minipumps, which were surgically implanted intraperitoneally. For DIO model, mice were fed ad libitum a chow diet (Ralston Purina Company) until 8 weeks of age and then placed ad libitum on a high fat/high sucrose (HF/HS) diet (Research Diets-D12266B, New Brunswick, NJ) with 16.8% kcal protein, 51.4% kcal carbohydrate, 31.8% kcal fat for an additional 8 weeks. For heart proteomic analysis, 8 to 12 weeks of age female HMDP mice (72 strains, n=2-3 mice; listed in Table S1) and 3 to 5 months old control and *Ndufs4*-cKO mice of both sex (n=5 each group) fed with chow diet ad libitum (Purina 5053, LabDiet) were used. All mice were maintained on a 14 h light/10 h dark cycle (light is on between 6 a.m. and 8 p.m.) at a temperature of 25 degrees and 30-70% humidity. On the day of the experiment, the mice were sacrificed after 4-hour fasting.

Heart global proteomic analysis

Heart tissue from the HMDP, control and *Ndufs4*-cKO mice were lysed in 6 M guanidine HCL (Sigma; #G4505), 100 mM Tris pH 8.5 containing 10 mM tris(2-carboxyethyl)phosphine (Sigma; #75259) and 40 mM 2-chloroacetamide (Sigma; #22790) by tip-probe sonication. The lysate was heated at 95°C for 5 min and centrifuged at 20,000 x g for 10 min at 4°C. The supernatant was diluted 1:1 with water and precipitated overnight with five volumes of acetone at -20°C. The lysate was centrifuged at 4,000 x g for 5 min at 4°C and the protein pellet was washed with 80% acetone. The lysate was centrifuged at 4,000 x g for 5 min at 4°C and the protein pellet was resuspended in Digestion Buffer (10% 2,2,2-Trifluoroethanol [Sigma; #96924] in 100 mM HEPEs pH 8.5). Protein was quantified with BCA (ThermoFisher Scientific) and normalized in Digestion Buffer to a final concentration of 2 µg/µl. Protein was digested with sequencing grade trypsin (Sigma; #T6567) and sequencing grade LysC (Wako; #129-02541) at a 1:50 enzyme:substrate ratio overnight at 37°C with shaking at 2000 x rpm. Eight micrograms of peptide was directly labelled with 32 µg of 10-plex TMT (lot #QB211242) in 20 µl at a final

concentration of 50% acetonitrile for 1.5 h at room temperature. The reaction was de-acylated with a final concentration of 0.3% (w/v) hydroxylamine and quenched with a final concentration of 1% trifluoroacetic acid (TFA). Each 10-plex experiment contained nine different strains with a tenth reference label (131 isobaric label) made up of the same peptide digest from pooled mix of C57BL/6J heart. Following labelling, the peptides from each of the 18 TMT 10-plex batches were pooled and purified directly by Styrene Divinylbenzene - Reversed-Phase Sulfonate (SDB-RPS) microcolumns, washed with 99% isopropanol containing 1% TFA and eluted with 80% acetonitrile containing 2% ammonium hydroxide followed by vacuum concentration. Peptides were resuspended in 2% acetonitrile containing 0.1% TFA and thirty micrograms of peptide was fractionated on an in-house fabricated 25 cm x 320 µm column packed with C18BEH particles (3 µm, Waters). Peptides were separated on a gradient of 0 – 30% acetonitrile containing 10 mM ammonium formate (pH 7.9) over 60 min at 6 µl/min using an Agilent 1260 HPLC and detection at 210 nm with a total of 48 fractions collected and concatenated down to 12 fractions.

Mass spectrometry and data processing

Peptide fractions from heart were resuspended in 2% acetonitrile containing 0.1% TFA and analyzed on a Dionex ultra-high pressure liquid chromatography system coupled to an Orbitrap Lumos mass spectrometer. Briefly, peptides were separated on 40 cm x 75 µm column containing 1.9 um C18AQ Reprosil particles on a linear gradient of 2-30% acetonitrile over 2 h. Electrospray ionization was performed at 2.3 kV with 40% RF lens and positively charged peptides detected via a full scan MS (350-1550 m/z, 1e6 AGC, 60K resolution, 50 ms injection time) followed data-dependent MS/MS analysis performed with CID of 35% normalized collision energy (NCE) (rapid scan rate, 2e4 AGC, 50 ms injection time, 10 ms activation time, 0.7 m/z isolation) of the top 10 most abundant peptides. Synchronous-precursor selection with MS3 (SPS-MS3) analysis was enabled with HCD of 60 NCE (100-500 m/z, 50K resolution, 1e5 AGC, 105 ms injection time) (72). Dynamic exclusion was enabled for 60 s. Data were processed with Proteome Discoverer v2.3 and searched against the Mouse UniProt database (November 2018) using SEQUEST (73). The precursor MS tolerance were set to 20 ppm and the MS/MS tolerance was set to 0.8 Da with a maximum of 2 miss-cleavage. The peptides were searched with oxidation of methionine set as variable modification, and TMT tags on peptide N-terminus / lysine and carbamidomethylation of cysteine set as a fixed modification. All data was

searched as a single batch and the peptide spectral matches (PSMs) of each database search filtered to 1% FDR using a target/decoy approach with Percolator (74). The filtered PSMs from each database search were grouped and q-values generated at the peptide level with the Qvality algorithm (75). Finally, the grouped peptide data was further filtered to 1% protein FDR using Protein Validator. Quantification was performed with the reporter ion quantification node for TMT quantification based on MS3 scans in Proteome Discoverer. TMT precision was set to 20 ppm and corrected for isotopic impurities. Only spectra with <50% co-isolation interference were used for quantification with an average signal-to-noise filter of >10. The data was filtered to retain Master proteins that were measured in at least 50 mice.

HMDP heart mRNA and miRNA expression analysis

Using the miRNeasy Mini Kit (QIAGEN), total RNA was extracted from HMDP heart tissues. From this, global mRNA expression were analyzed as previously described (76), while the QIAseq miRNA Library Kit (QIAGEN) was used to create miRNA libraries. These libraries were then sequenced using 1x50 HiSeq sequencing. Reads were mapped using hisat2 (version 2.0.6) and counted using htseq-count (version 0.13.5). Differential expression analysis was performed with DESeq2.

Association mapping

Genotypes for the mouse strains were obtained using the Mouse Diversity Array (77). After filtering for quality or missing genotypes, about 200,000 remained. Genome-wide association for phenotypes and protein abundance levels was performed using Factored Spectrally Transformed Linear Mixed Models (FaST-LMM), which applies a linear mixed model to correct for population structure (78). A cutoff value for genome-wide significance was set at 4.1E-06, as determined previously (77).

Cell culture and treatments

Following isolation, neonatal rat ventricular myocytes (NRVMs) were plated in DMEM containing 10% Fetal bovine serum (FBS) and 1% antibiotics overnight. The next day, NRVMs were changed to serum-free medium in the presence or absence of 100 μM phenylephrine (Sigma, Cat# P6126-10G). The cells were then transfected with miRNA control, mature *miR-*

448 *27b-5p*, or *miR-27b-3p* mimics (Sigma) for 48 h. The cell lysates were harvested for
449 immunoblotting using primary antibodies against NDUFS4 (# sc-100567, Santa Cruz) and Actin
450 (# 8457S, Cell Signaling). Band densitometry was quantified using ImageJ Gel Plugin (NIH).

Reagent	Mature sequence 5' to 3'
MISSION® microRNA, Negative Control 1 (miRNA control)	GGUUCGUACGUACACUGUUCA
MISSION® microRNA - hsa-miR-27b* (miR-27b-5p)	AGAGCUUAGCUGAUUGGUGAAC
MISSION® microRNA - hsa-miR-27b (miR-27b-3p)	UUCACAGUGGCUAAGUUCUGC

451

452 **Mitochondria isolation from frozen hearts**

453 20 mg of frozen hearts were thawed in 1.4 mL of ice-cold isolation buffer (70 mM sucrose, 220
454 mM mannitol, 1 mM EGTA, 2 mM HEPES, pH 7.4 containing protease inhibitors). Hearts were
455 mechanically homogenized with 20 strokes of a Dounce homogenizer at 4°C. Homogenates were
456 centrifuged at 1,000 g for 10 min at 4˚C. Supernatant was collected (300 µL were reserved as
457 whole lysate) and centrifuged at 10,000 g for 10 min at 4˚C to obtain a pellet containing the
458 mitochondria. Mitochondrial pellet was re-suspended in 1 mL of isolation buffer and re-
459 centrifuged at 10,000 g for 10 min at 4˚C. The mitochondrial pellet was finally re-suspended in
460 200 µL of isolation buffer and protein concentration determined using the BCA assay.

461

462 **CoQ extraction from whole lysate and mitochondrial enriched fractions**

463 CoQ extraction, detection and analysis was performed as described previously (79). Briefly, 15
464 µg protein from mitochondrial fractions or 200 µg protein from total lysate were aliquoted into 2
465 mL Eppendorf tubes and volumes adjusted to 100 µL for mitochondrial fractions or 200 µL for
466 whole lysates, and samples were kept on ice for the entire process. 20 µL of 0.1 ng/mL CoQ8 (2
467 ng total; Avanti Polar Lipids) were added to each sample as an internal standard. To protein
468 aliquots ice-cold 250 µL acidified methanol (0.1% HCl in MeOH) were added to each sample,
469 followed by 300 µL hexane and samples were thoroughly mixed by vertexing. Hexane and
470 MeOH/water layers were separated by centrifugation at 15,000 g for 5 min at 4˚C. The upper
471 layer of hexane was collected and transferred to clean 2 mL Eppendorf tubes and completely

dried in a GeneVac vacuum centrifuge, on a low BP point method for 40 mins (20 min pre-final stage and 20 min final stage). Samples were reconstituted in 100 µL ethanol before analysis of CoQ levels by LC-MS.

LC-MS analysis of CoQ

CoQ8, 9 and 10 levels were analyzed using a TSQ Altis triple quadrupole mass spectrometer (ThermoFisher) coupled to a Vanquish LC system (ThermoFisher). 15 µL of sample was injected and separated on a 2.6 µm Kinetex XB-C18 100 A column (50 × 2.10 mm; Phenomenex) at 45˚C. Mobile Phase A consisted of 2.5 mM ammonium formate in 95 % MeOH, 5 % IPA and Mobile Phase B consisted of 2.4 mm ammonium formate in 100 % IPA. A gradient method over 5 min was used with an initial concentration of 0 % B held for 1 min before increased to 45 % B over 1 min and held for 1 min, before decreasing back to 0 % B over 0.5 min and column re-equilibrated over 1.5 min. Eluent was then directed into the QQQ with the following settings: source voltage = 3500 V; sheath gas 2; aux gas 2; transfer capillary temperature = 350 ˚C. Ammonium adducts of each of the analytes were detected by SRM with Q1 and Q3 resolution set to 0.7 FWHM with the following parameters: $[CoQ8+NH4]^+$, *m/z* 744.9 → 197.1 with collision energy 32.76; $[CoQ9+NH4]^+$, *m/z* 812.9 → 197.1 with collision energy 32.76; $[CoQ9H_2+NH4]^+$, *m/z* 814.9 → 197.1 with collision energy 36.4; $[CoQ10+NH4]^+$, *m/z* 880.9 → 197.1 with collision energy 32.76; and $[CoQ10H_2+NH4]^+$, *m/z* 882.9 → 197.1 with collision energy 36.4. CoQ9 and CoQ10 were quantified in samples against a standard curve (0 – 1000 nM) and normalized to spiked in CoQ8 levels (20 ng/mL) in each sample and standard. No $CoQ9H_2$ and $CoQ10H_2$ were detected in any of the samples, though some bleed through into these channels was detected for the oxidized analytes, though these are resolved from the reduced standard peaks (as reported previously).

Data availability

All sequencing raw data can be accessed at the Gene Expression Omnibus under accession GSE194198 (HF/HS heart HMDP RNA-seq data) and GSE207142 (HF/HS heart HMDP miRNA-seq data).

Statistical analysis

Statistical analyses were performed using Prism v9.4.0 (GraphPad Software, Inc., La Jolla, CA, USA). Errors bars plotted on graphs are presented as the mean ± SEM unless reported otherwise. The critical significance value (α) was set at 0.05, and if the P values were less than α, we reported that the observed differences were statistically significant. Correlations were calculated using biweight midcorrelation using the bicorAndPvalue function of the WGCNA package (29).

AUTHOR CONTRIBUTIONS

K.C.K. and A.J.L. conceived the study. K.C.K. generated, analyzed, and interpreted the data, and prepared the figures. L.C., A.D.V. and D.E.J. generated, analyzed, and interpreted the CoQ analyses. C.L., and C.F.L. bred, genotyped, and harvested the hearts from the *Ndufs4*-cKO animals. M.M.S., B.L.P. and D.E.J. generated, analyzed, and interpreted the proteomic datasets. E.J.E.H. performed WGCNA analyses. C.P. carried out mRNA sequencing analysis. K.E.K.U. and M.P. carried out miRNA sequencing analysis. V.S., D.A. and Y.C. performed *in vitro* studies. K.C.K. and A.J.L. drafted the manuscript, and all authors read or revised the manuscript.

SOURCES OF FUNDING

This work was supported by NIH grants DK120342, HL148577 and HL147883 (A.J.L.) and DOD grant W81XWH2110115 (A.J.L.); R00DK120875 (K.C.K); R00HL138193 (M.M.S.); National Health and Medical Research Council of Australia (NHMRC) grants and fellowships (D.E.J. and B.L.P.); Systems Biology Association fellowship, Foundation Sorbonne fellowship, French Minister, and Master BIP (E.J.E.H.). The funders had no role in study design, data collection and interpretation, or the decision to submit the work for publication.

DISCLOSURES

None.

FIGURE LEGENDS

Figure 1. Genetic architecture of heart mitochondrial proteome.

(A) High-resolution association mapping of 840 heart mitochondrial proteins from 72 HMDP strains to identify pQTL networks. Associations between protein abundance levels and genetic variants located within 1Mb of the respective gene location were considered as *cis*-pQTLs (P < 1E-05) shown along the diagonal axis and the rest were considered as *trans*-pQTLs (P < 1E-06). Three *trans*-pQTL hotspots are indicated by arrows. **(B)** Five WGCNA modules and the respective *trans*-pQTL hotspots are shown. HMDP, hybrid mouse diversity panel; pQTL, protein quantitative trait locus; WGCNA, weighted gene co-expression network analysis.

Figure 2. Chr13 locus controls mitochondrial complex-I *via miR-27b*/NDUFS4 axis.

(A) Circos plot showing chr13 hotspot. Each line signifies a significant association between the genetic variants and the respective protein levels with candidate genes being highlighted. **(B)** Manhattan and regional plots of chr13 locus (brown module) eigengene, respectively. Red line signifies genome-wide significance threshold (P < 4.1E-06). The peak SNPs and the candidate genes are highlighted. Genotype distribution plots of **(C)** protein levels and eigengenes, and cardiac phenotypes from **(D)** ISO-induced HF model and **(E)** female and **(F)** male DIO model at peak SNP (rs48592660) associated with chr13 locus. **(G)** Volcano plot showing differentially expressed protein levels between control and heart-specific *Ndufs4*-cKO mice (n = 5 mice/group). Significantly different proteins (significance cutoff: abs[$\log_2$FC] > 1 and P_{adj} < 0.001) are highlighted in red. **(H)** Genotype distribution plots of heart *miR-27b* expression at peak SNP (rs48592660) associated with chr13 locus. **(I)** Gene-by-trait correlation plot between heart weight phenotype and heart *miR-27b* expression. **(J)** Immunoblot analyses of NDUFS4 protein levels in NRVMs transfected with mature *miR-27b* in the presence or absence of PE treatment. Data are presented as **(C – F and H)** boxplots showing median and interquartile range with outliers shown as circles (n = 68-72 strains for protein levels; n = 92-95 strains for ISO-model; n = 92-100 strains for DIO-model; n = 85 strains for miRNA levels) or **(J)** mean ± SEM (n = 2-4 per group). *P* values were calculated using **(A and B)** FaST-LMM that uses Likelihood-Ratio test; **(C – F and H)** Unpaired two-tailed Student's t test; **(I)** BicorAndPvalue function of the WGCNA R-package that uses Unpaired two-tailed Student's t test; **(J)** 2-factor ANOVA corrected by post-hoc "Holm-Sidak's" multiple comparisons test. ISO, isoproterenol; HF, heart

failure; DIO, diet-induced obesity; NRVMs, neonatal rat ventricular myocytes; PE, phenylephrine.

Figure 3. Chr17 locus controls mitoribosomes *via* LRPPRC/SLIRP.

(A) Circos plot showing chr17 hotspot. Each line signifies a significant association between the genetic variants and the respective protein levels with candidate genes being highlighted. **(B)** Manhattan and regional plots of chr17 locus (green module) eigengene, respectively. Red line signifies genome-wide significance threshold (P < 4.1E-06). The peak SNPs and the candidate genes are highlighted. Genotype distribution plots of **(C)** protein levels and eigengenes, and cardiac phenotypes from **(D)** ISO-induced HF model and **(E)** female and **(F)** male DIO model at peak SNP (rs46340181) associated with chr17 locus. **(G)** Protein-by-protein correlation plot between heart LRPPRC and SLIRP abundance levels. **(H)** Association *P* values between mtDNA-encoded mRNA expression or protein abundance levels and peak SNP (rs46340181) associated with chr17 locus in both sexes of HMDP. **(I)** Genotype distribution plots of heart *mt-ND1* mRNA expression from female and male DIO model at peak SNPs associated with chr17 (rs46340181) or chr13 (rs48592660) loci, respectively. **(J)** Association *P* values between mtDNA-encoded complex-I related mRNA expression or protein abundance levels and peak SNP (rs48592660) associated with chr13 locus in both sexes of HMDP. Data are presented as **(C – F and I)** boxplots showing median and interquartile range with outliers shown as circles (n = 68-72 strains for protein levels; n = 92-95 strains for ISO-model; n = 92-100 strains for DIO-model). *P* values were calculated using **(A, B, H and J)** FaST-LMM that uses Likelihood-Ratio test; **(C – F and I)** Unpaired two-tailed Student's t test; **(G)** BicorAndPvalue function of the WGCNA R-package that uses Unpaired two-tailed Student's t test.

Figure 4. Chr7 locus affects CoQ metabolism *via* COQ7.

(A) Circos plot showing chr7 hotspot. Each line signifies a significant association between the genetic variants and the respective protein levels with candidate genes being highlighted. **(B)** Manhattan and regional plots of chr7 locus (turquoise module) eigengene, respectively. Red line signifies genome-wide significance threshold (P < 4.1E-06). The peak SNPs and the candidate genes are highlighted. Genotype distribution plots of **(C)** protein levels and eigengenes, and cardiac phenotypes from **(D)** ISO-induced HF model and **(E)** female and **(F)** male DIO model at

peak SNP (rs32451909) associated with chr7 locus. Protein-by-protein correlation plots between heart COQ7 and **(G)** COQ3, **(H)** COQ6 and **(I)** COQ9 abundance levels. **(J)** Genotype distribution plots of CoQ9 or CoQ10 levels in both the mitochondrial fractions and total heart lysates from female DIO model at peak SNPs associated with chr7 (rs32451909) locus. Data are presented as **(C – F and J)** boxplots showing median and interquartile range with outliers shown as circles (n = 68-72 strains for protein levels; n = 92-95 strains for ISO-model; n = 92-100 strains for DIO-model; n = 15 strains for CoQ9 and CoQ10 levels). *P* values were calculated using **(A and B)** FaST-LMM that uses Likelihood-Ratio test; **(C – F and J)** Unpaired two-tailed Student's t test; **(G – I)** BicorAndPvalue function of the WGCNA R-package that uses Unpaired two-tailed Student's t test.

SOURCE DATA LEGENDS

Figure 2 – source data 1. Uncropped blots for Figure 2, panel J.

Uncropped immunoblots probed for NDUFS4 (left) and ACTIN (right) protein levels in NRVMs transfected with mature *miR-27b* in the presence or absence of PE treatment. Corresponding molecular weight markers are labelled on the right side of each blot.

REFERENCES

1. Yin X, Lanza IR, Swain JM, Sarr MG, Nair KS, Jensen MD. Adipocyte mitochondrial function is reduced in human obesity independent of fat cell size. J Clin Endocrinol Metab. 2014;99(2):E209-16.

2. Chouchani ET, Methner C, Buonincontri G, Hu CH, Logan A, Sawiak SJ, et al. Complex I deficiency due to selective loss of Ndufs4 in the mouse heart results in severe hypertrophic cardiomyopathy. PLoS One. 2014;9(4):e94157.

3. Begriche K, Igoudjil A, Pessayre D, Fromenty B. Mitochondrial dysfunction in NASH: causes, consequences and possible means to prevent it. Mitochondrion. 2006;6(1):1-28.

4. Sanyal AJ, Campbell-Sargent C, Mirshahi F, Rizzo WB, Contos MJ, Sterling RK, et al. Nonalcoholic steatohepatitis: association of insulin resistance and mitochondrial abnormalities. Gastroenterology. 2001;120(5):1183-92.

5. Kim JA, Wei Y, Sowers JR. Role of mitochondrial dysfunction in insulin resistance. Circ Res. 2008;102(4):401-14.

6. Wallace DC. Mitochondrial genetic medicine. Nature genetics. 2018;50(12):1642-9.

7. Murphy E, Ardehali H, Balaban RS, DiLisa F, Dorn GW, 2nd, Kitsis RN, et al. Mitochondrial Function, Biology, and Role in Disease: A Scientific Statement From the American Heart Association. Circ Res. 2016;118(12):1960-91.

8. Brown DA, Perry JB, Allen ME, Sabbah HN, Stauffer BL, Shaikh SR, et al. Expert consensus document: Mitochondrial function as a therapeutic target in heart failure. Nat Rev Cardiol. 2017;14(4):238-50.

9. Zhou B, Tian R. Mitochondrial dysfunction in pathophysiology of heart failure. J Clin Invest. 2018;128(9):3716-26.

10. Civelek M, Lusis AJ. Systems genetics approaches to understand complex traits. Nat Rev Genet. 2014;15(1):34-48.

11. Seldin M, Yang X, Lusis AJ. Systems genetics applications in metabolism research. Nat Metab. 2019;1(11):1038-50.

12. Lusis AJ, Seldin MM, Allayee H, Bennett BJ, Civelek M, Davis RC, et al. The Hybrid Mouse Diversity Panel: a resource for systems genetics analyses of metabolic and cardiovascular traits. J Lipid Res. 2016;57(6):925-42.

13. Parks BW, Nam E, Org E, Kostem E, Norheim F, Hui ST, et al. Genetic control of obesity and gut microbiota composition in response to high-fat, high-sucrose diet in mice. Cell Metab. 2013;17(1):141-52.

14. Parks BW, Sallam T, Mehrabian M, Psychogios N, Hui ST, Norheim F, et al. Genetic architecture of insulin resistance in the mouse. Cell Metab. 2015;21(2):334-47.

15. Rau CD, Wang J, Avetisyan R, Romay MC, Martin L, Ren S, et al. Mapping genetic contributions to cardiac pathology induced by Beta-adrenergic stimulation in mice. Circ Cardiovasc Genet. 2015;8(1):40-9.

16. Org E, Mehrabian M, Parks BW, Shipkova P, Liu X, Drake TA, et al. Sex differences and hormonal effects on gut microbiota composition in mice. Gut Microbes. 2016;7(4):313-22.

17. Wang JJ, Rau C, Avetisyan R, Ren S, Romay MC, Stolin G, et al. Genetic Dissection of Cardiac Remodeling in an Isoproterenol-Induced Heart Failure Mouse Model. PLoS Genet. 2016;12(7):e1006038.

18. Seldin MM, Kim ED, Romay MC, Li S, Rau CD, Wang JJ, et al. A systems genetics approach identifies Trp53inp2 as a link between cardiomyocyte glucose utilization and hypertrophic response. American journal of physiology Heart and circulatory physiology. 2017;312(4):H728-H41.

19. Rau CD, Romay MC, Tuteryan M, Wang JJ, Santolini M, Ren S, et al. Systems Genetics Approach Identifies Gene Pathways and Adamts2 as Drivers of Isoproterenol-Induced Cardiac Hypertrophy and Cardiomyopathy in Mice. Cell systems. 2017;4(1):121-8.e4.

20. Norheim F, Hui ST, Kulahcioglu E, Mehrabian M, Cantor RM, Pan C, et al. Genetic and hormonal control of hepatic steatosis in female and male mice. J Lipid Res. 2017;58(1):178-87.

21. Norheim F, Bjellaas T, Hui ST, Chella Krishnan K, Lee J, Gupta S, et al. Genetic, dietary, and sex-specific regulation of hepatic ceramides and the relationship between hepatic ceramides and IR. Journal of lipid research. 2018;59(7):1164-74.

22. Hui ST, Kurt Z, Tuominen I, Norheim F, R CD, Pan C, et al. The Genetic Architecture of Diet-Induced Hepatic Fibrosis in Mice. Hepatology. 2018;68(6):2182-96.

23. Seldin MM, Koplev S, Rajbhandari P, Vergnes L, Rosenberg GM, Meng Y, et al. A Strategy for Discovery of Endocrine Interactions with Application to Whole-Body Metabolism. Cell Metab. 2018;27(5):1138-55 e6.

671 24. Chella Krishnan K, Kurt Z, Barrere-Cain R, Sabir S, Das A, Floyd R, et al. Integration of
672 Multi-omics Data from Mouse Diversity Panel Highlights Mitochondrial Dysfunction in Non-
673 alcoholic Fatty Liver Disease. Cell Syst. 2018;6(1):103-15 e7.
674 25. Chella Krishnan K, Sabir S, Shum M, Meng Y, Acin-Perez R, Lang JM, et al. Sex-
675 specific metabolic functions of adipose Lipocalin-2. Mol Metab. 2019;30:30-47.
676 26. Norheim F, Hasin-Brumshtein Y, Vergnes L, Chella Krishnan K, Pan C, Seldin MM, et
677 al. Gene-by-Sex Interactions in Mitochondrial Functions and Cardio-Metabolic Traits. Cell
678 Metab. 2019;29(4):932-49 e4.
679 27. Chella Krishnan K, Vergnes L, Acin-Perez R, Stiles L, Shum M, Ma L, et al. Sex-specific
680 genetic regulation of adipose mitochondria and metabolic syndrome by *Ndufv2*. Nat Metab.
681 2021;3(11):1552-68.
682 28. Calvo SE, Clauser KR, Mootha VK. MitoCarta2.0: an updated inventory of mammalian
683 mitochondrial proteins. Nucleic Acids Res. 2016;44(D1):D1251-7.
684 29. Langfelder P, Horvath S. WGCNA: an R package for weighted correlation network
685 analysis. BMC Bioinformatics. 2008;9(1):559.
686 30. Huang da W, Sherman BT, Lempicki RA. Systematic and integrative analysis of large
687 gene lists using DAVID bioinformatics resources. Nat Protoc. 2009;4(1):44-57.
688 31. Wang J, Song Y, Zhang Y, Xiao H, Sun Q, Hou N, et al. Cardiomyocyte overexpression
689 of miR-27b induces cardiac hypertrophy and dysfunction in mice. Cell Res. 2012;22(3):516-27.
690 32. Wang Y, Cai H, Li H, Gao Z, Song K. Atrial overexpression of microRNA-27b
691 attenuates angiotensin II-induced atrial fibrosis and fibrillation by targeting ALK5. Hum Cell.
692 2018;31(3):251-60.
693 33. Zhu J, Vinothkumar KR, Hirst J. Structure of mammalian respiratory complex I. Nature.
694 2016;536(7616):354-8.
695 34. Stroud DA, Surgenor EE, Formosa LE, Reljic B, Frazier AE, Dibley MG, et al.
696 Accessory subunits are integral for assembly and function of human mitochondrial complex I.
697 Nature. 2016;538(7623):123-6.
698 35. Gu J, Wu M, Guo R, Yan K, Lei J, Gao N, et al. The architecture of the mammalian
699 respirasome. Nature. 2016;537(7622):639-43.

36. Kahlhöfer F, Kmita K, Wittig I, Zwicker K, Zickermann V. Accessory subunit NUYM (NDUFS4) is required for stability of the electron input module and activity of mitochondrial complex I. Biochimica Et Biophysica Acta Bba - Bioenergetics. 2017;1858(2):175-81.

37. Scacco S, Petruzzella V, Budde S, Vergari R, Tamborra R, Panelli D, et al. Pathological mutations of the human NDUFS4 gene of the 18-kDa (AQDQ) subunit of complex I affect the expression of the protein and the assembly and function of the complex. J Biol Chem. 2003;278(45):44161-7.

38. Leshinsky-Silver E, Lebre AS, Minai L, Saada A, Steffann J, Cohen S, et al. NDUFS4 mutations cause Leigh syndrome with predominant brainstem involvement. Mol Genet Metab. 2009;97(3):185-9.

39. Karamanlidis G, Lee CF, Garcia-Menendez L, Kolwicz SC, Jr., Suthammarak W, Gong G, et al. Mitochondrial complex I deficiency increases protein acetylation and accelerates heart failure. Cell Metab. 2013;18(2):239-50.

40. Zhang H, Gong G, Wang P, Zhang Z, Kolwicz SC, Rabinovitch PS, et al. Heart specific knockout of Ndufs4 ameliorates ischemia reperfusion injury. J Mol Cell Cardiol. 2018;123:38-45.

41. Adjobo-Hermans MJW, de Haas R, Willems P, Wojtala A, van Emst-de Vries SE, Wagenaars JA, et al. NDUFS4 deletion triggers loss of NDUFA12 in Ndufs4(-/-) mice and Leigh syndrome patients: A stabilizing role for NDUFAF2. Biochim Biophys Acta Bioenerg. 2020;1861(8):148213.

42. Leong DW, Komen JC, Hewitt CA, Arnaud E, McKenzie M, Phipson B, et al. Proteomic and metabolomic analyses of mitochondrial complex I-deficient mouse model generated by spontaneous B2 short interspersed nuclear element (SINE) insertion into NADH dehydrogenase (ubiquinone) Fe-S protein 4 (Ndufs4) gene. J Biol Chem. 2012;287(24):20652-63.

43. Siira SJ, Spahr H, Shearwood AJ, Ruzzenente B, Larsson NG, Rackham O, et al. LRPPRC-mediated folding of the mitochondrial transcriptome. Nat Commun. 2017;8(1):1532.

44. Chujo T, Ohira T, Sakaguchi Y, Goshima N, Nomura N, Nagao A, et al. LRPPRC/SLIRP suppresses PNPase-mediated mRNA decay and promotes polyadenylation in human mitochondria. Nucleic Acids Res. 2012;40(16):8033-47.

729 45. Ruzzenente B, Metodiev MD, Wredenberg A, Bratic A, Park CB, Camara Y, et al.
730 LRPPRC is necessary for polyadenylation and coordination of translation of mitochondrial
731 mRNAs. EMBO J. 2012;31(2):443-56.
732 46. Mootha VK, Lepage P, Miller K, Bunkenborg J, Reich M, Hjerrild M, et al. Identification
733 of a gene causing human cytochrome c oxidase deficiency by integrative genomics. Proc Natl
734 Acad Sci U S A. 2003;100(2):605-10.
735 47. Olahova M, Hardy SA, Hall J, Yarham JW, Haack TB, Wilson WC, et al. LRPPRC
736 mutations cause early-onset multisystem mitochondrial disease outside of the French-Canadian
737 population. Brain. 2015;138(Pt 12):3503-19.
738 48. Sharma A, Fonarow GC, Butler J, Ezekowitz JA, Felker GM. Coenzyme Q10 and Heart
739 Failure: A State-of-the-Art Review. Circ Heart Fail. 2016;9(4):e002639.
740 49. Yao C, Chen G, Song C, Keefe J, Mendelson M, Huan T, et al. Genome-wide mapping of
741 plasma protein QTLs identifies putatively causal genes and pathways for cardiovascular disease.
742 Nature communications. 2018;9(1):3268.
743 50. Ruffieux H, Carayol J, Popescu R, Harper ME, Dent R, Saris WHM, et al. A fully joint
744 Bayesian quantitative trait locus mapping of human protein abundance in plasma. Plos Comput
745 Biol. 2020;16(6):e1007882.
746 51. Zhong W, Gummesson A, Tebani A, Karlsson MJ, Hong MG, Schwenk JM, et al.
747 Whole-genome sequence association analysis of blood proteins in a longitudinal wellness cohort.
748 Genome Med. 2020;12(1):53.
749 52. Yang C, Farias FHG, Ibanez L, Suhy A, Sadler B, Fernandez MV, et al. Genomic atlas of
750 the proteome from brain, CSF and plasma prioritizes proteins implicated in neurological
751 disorders. Nat Neurosci. 2021;24(9):1302-12.
752 53. Folkersen L, Gustafsson S, Wang Q, Hansen DH, Hedman AK, Schork A, et al. Genomic
753 and drug target evaluation of 90 cardiovascular proteins in 30,931 individuals. Nat Metab.
754 2020;2(10):1135-48.
755 54. He B, Shi J, Wang X, Jiang H, Zhu HJ. Genome-wide pQTL analysis of protein
756 expression regulatory networks in the human liver. Bmc Biol. 2020;18(1):97.
757 55. Aguet F, Brown AA, Castel SE, Davis JR, He Y, Jo B, et al. Genetic effects on gene
758 expression across human tissues. Nature. 2017;550(7675):204-13.

759 56. Brynedal B, Choi J, Raj T, Bjornson R, Stranger BE, Neale BM, et al. Large-Scale trans-
760 eQTLs Affect Hundreds of Transcripts and Mediate Patterns of Transcriptional Co-regulation.
761 Am J Hum Genet. 2017;100(4):581-91.
762 57. Yao C, Joehanes R, Johnson AD, Huan T, Liu C, Freedman JE, et al. Dynamic Role of
763 trans Regulation of Gene Expression in Relation to Complex Traits. Am J Hum Genetics.
764 2017;100(4):571-80.
765 58. Small KS, Todorčević M, Civelek M, Moustafa JSE-S, Wang X, Simon MM, et al.
766 Regulatory variants at KLF14 influence type 2 diabetes risk via a female-specific effect on
767 adipocyte size and body composition. Nature genetics. 2018;50(4):572-80.
768 59. Consortium TG. The GTEx Consortium atlas of genetic regulatory effects across human
769 tissues. Science. 2020;369(6509):1318-30.
770 60. Fiedorczuk K, Letts JA, Degliesposti G, Kaszuba K, Skehel M, Sazanov LA. Atomic
771 structure of the entire mammalian mitochondrial complex I. Nature. 2016;538(7625):406-10.
772 61. Hirst J. Mitochondrial complex I. Annu Rev Biochem. 2013;82(1):551-75.
773 62. Li G, Shao Y, Guo HC, Zhi Y, Qiao B, Ma K, et al. MicroRNA-27b-3p down-regulates
774 FGF1 and aggravates pathological cardiac remodelling. Cardiovasc Res. 2022;118(9):2139-51.
775 63. Yu J, Lv Y, Di W, Liu J, Kong X, Sheng Y, et al. MiR-27b-3p Regulation in Browning
776 of Human Visceral Adipose Related to Central Obesity: MiR-27b-3p in Browning of Human
777 VAT. Obesity. 2017;26(2):387-96.
778 64. Sun L, Trajkovski M. MiR-27 orchestrates the transcriptional regulation of brown
779 adipogenesis. Metabolis. 2014;63(2):272-82.
780 65. Kong X, Yu J, Bi J, Qi H, Di W, Wu L, et al. Glucocorticoids transcriptionally regulate
781 miR-27b expression promoting body fat accumulation via suppressing the browning of white
782 adipose tissue. Diabetes. 2015;64(2):393-404.
783 66. Nakai D, Yuasa S, Takahashi M, Shimizu T, Asaumi S, Isono K, et al. Mouse homologue
784 of coq7/clk-1, longevity gene in Caenorhabditis elegans, is essential for coenzyme Q synthesis,
785 maintenance of mitochondrial integrity, and neurogenesis. Biochem Bioph Res Co.
786 2001;289(2):463-71.
787 67. Wang Y, Oxer D, Hekimi S. Mitochondrial function and lifespan of mice with controlled
788 ubiquinone biosynthesis. Nat Commun. 2015;6(1):6393.

68. Lapointe J, Hekimi S. Early mitochondrial dysfunction in long-lived Mclk1+/- mice. J Biological Chem. 2008;283(38):26217-27.

69. Lapointe J, Stepanyan Z, Bigras E, Hekimi S. Reversal of the Mitochondrial Phenotype and Slow Development of Oxidative Biomarkers of Aging in Long-lived Mclk1+/− Mice. J Biol Chem. 2009;284(30):20364-74.

70. Liu X, Jiang N, Hughes B, Bigras E, Shoubridge E, Hekimi S. Evolutionary conservation of the clk-1-dependent mechanism of longevity: loss of mclk1 increases cellular fitness and lifespan in mice. Genes Dev. 2005;19(20):2424-34.

71. Lapointe J, Wang Y, Bigras E, Hekimi S. The submitochondrial distribution of ubiquinone affects respiration in long-lived Mclk1+/− mice. J Cell Biol. 2012;199(2):215-24.

72. McAlister GC, Nusinow DP, Jedrychowski MP, Wuhr M, Huttlin EL, Erickson BK, et al. MultiNotch MS3 enables accurate, sensitive, and multiplexed detection of differential expression across cancer cell line proteomes. Anal Chem. 2014;86(14):7150-8.

73. Eng JK, McCormack AL, Yates JR. An approach to correlate tandem mass spectral data of peptides with amino acid sequences in a protein database. J Am Soc Mass Spectrom. 1994;5(11):976-89.

74. Kall L, Canterbury JD, Weston J, Noble WS, MacCoss MJ. Semi-supervised learning for peptide identification from shotgun proteomics datasets. Nat Methods. 2007;4(11):923-5.

75. Kall L, Storey JD, Noble WS. QVALITY: non-parametric estimation of q-values and posterior error probabilities. Bioinformatics. 2009;25(7):964-6.

76. Cao Y, Vergnes L, Wang YC, Pan C, Chella Krishnan K, Moore TM, et al. Sex differences in heart mitochondria regulate diastolic dysfunction. Nat Commun. 2022;13(1):3850.

77. Bennett BJ, Farber CR, Orozco L, Kang HM, Ghazalpour A, Siemers N, et al. A high-resolution association mapping panel for the dissection of complex traits in mice. Genome Res. 2010;20(2):281-90.

78. Lippert C, Listgarten J, Liu Y, Kadie CM, Davidson RI, Heckerman D. FaST linear mixed models for genome-wide association studies. Nat Methods. 2011;8(10):833-5.

79. Burger N, Logan A, Prime TA, Mottahedin A, Caldwell ST, Krieg T, et al. A sensitive mass spectrometric assay for mitochondrial CoQ pool redox state in vivo. Free Radic Biol Med. 2020;147:37-47.

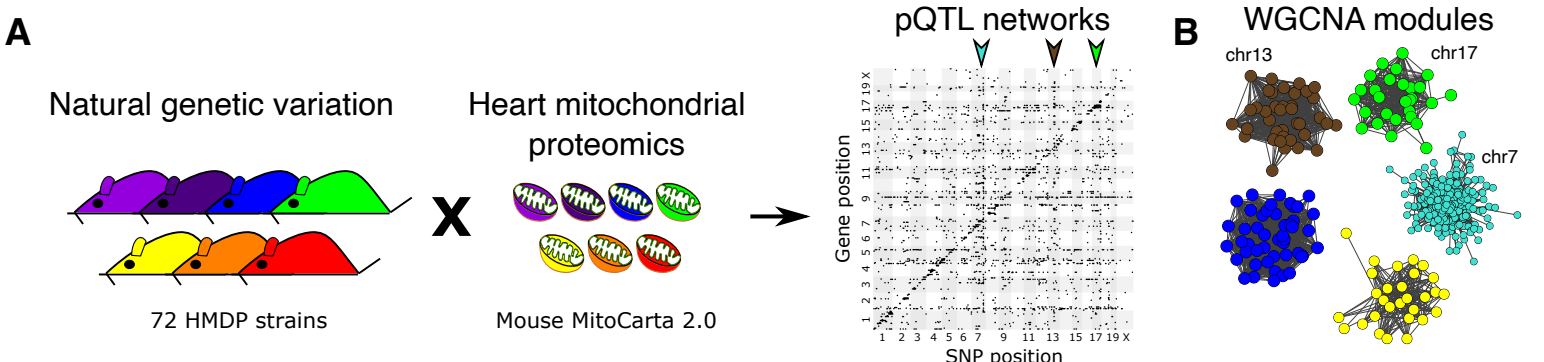
A
Natural genetic variation
72 HMDP strains
X
Heart mitochondrial proteomics
Mouse MitoCarta 2.0
pQTL networks
Gene position
SNP position
1 2 3 4 5 6 7 9 11 13 15 17 19 X
B
WGCNA modules
chr13
chr17
chr7

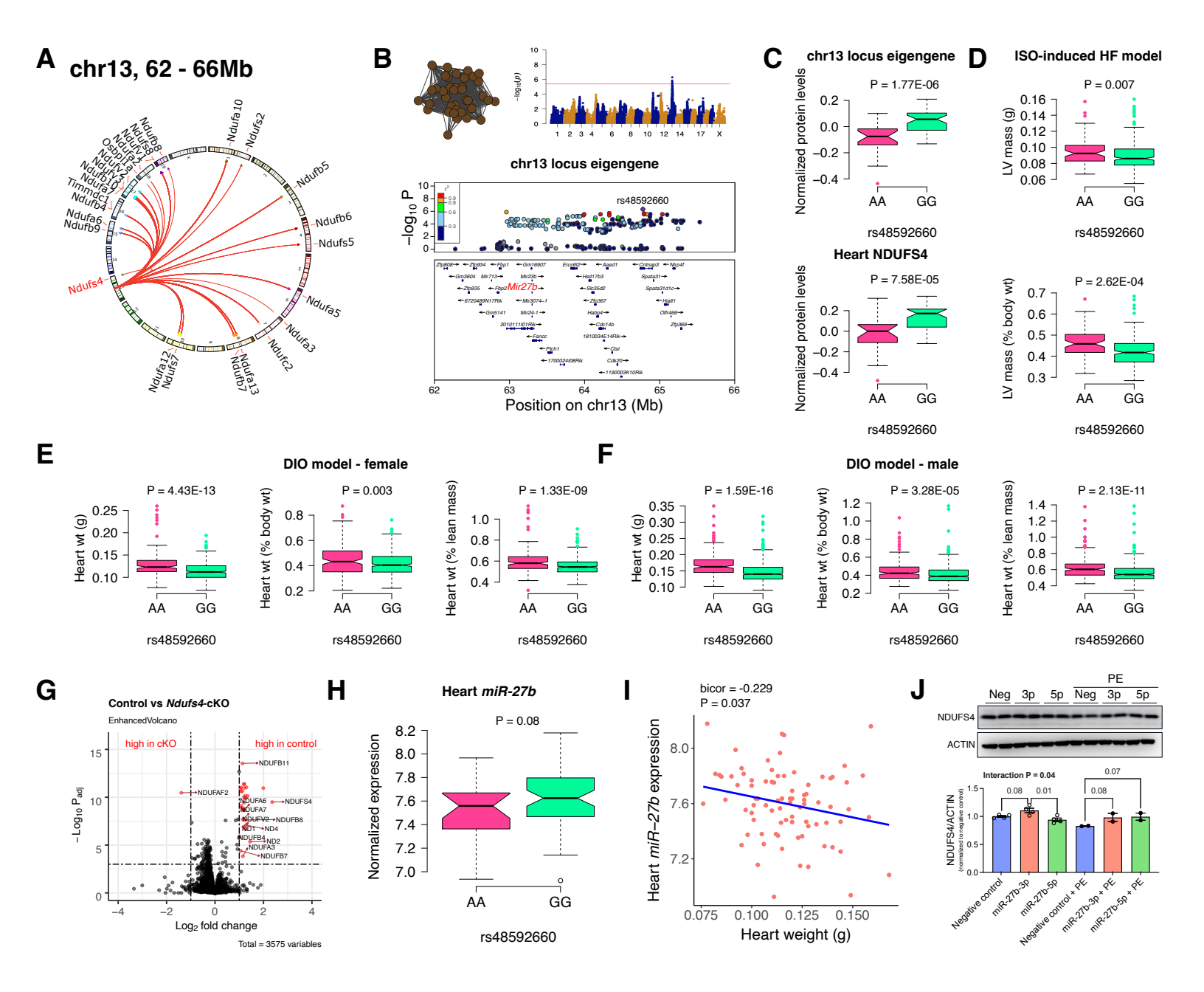
A
chr13, 62 - 66Mb
Ndufa10
Ndufs2
Ndufb5
Ndufb6
Ndufs5
Ndufa5
Ndufa3
Ndufc2
Ndufa13
Ndufb7
Ndufa12
Ndufs7
Ndufs4
Ndufa6
Ndufb9
Ndufb4
Timmdc1
Ndufb11
Ndufv2
Ndufa7
Ndufa2
Ndufb8
B
chr13 locus eigengene
rs48592660
Mir27b
Position on chr13 (Mb)
C
chr13 locus eigengene
P = 1.77E-06
Normalized protein levels
AA
GG
rs48592660
Heart NDUFS4
P = 7.58E-05
D
ISO-induced HF model
P = 0.007
LV mass (g)
P = 2.62E-04
LV mass (% body wt)
E
DIO model - female
P = 4.43E-13
Heart wt (g)
P = 0.003
Heart wt (% body wt)
P = 1.33E-09
Heart wt (% lean mass)
F
DIO model - male
P = 1.59E-16
P = 3.28E-05
P = 2.13E-11
G
Control vs Ndufs4-cKO
EnhancedVolcano
high in cKO
high in control
NDUFB11
NDUFAF2
NDUFA6
NDUFS4
NDUFA7
NDUFV2
NDUFB6
ND1
ND4
NDUFB4
ND2
NDUFA3
NDUFB7
−Log10 Padj
Log2 fold change
Total = 3575 variables
H
Heart miR-27b
P = 0.08
Normalized expression
I
bicor = -0.229
P = 0.037
Heart miR−27b expression
Heart weight (g)
J
Neg
3p
5p
PE
NDUFS4
ACTIN
Interaction P = 0.04
NDUFS4/ACTIN
(normalized to negative control)
Negative control
miR-27b-3p
miR-27b-5p
Negative control + PE
miR-27b-3p + PE
miR-27b-5p + PE

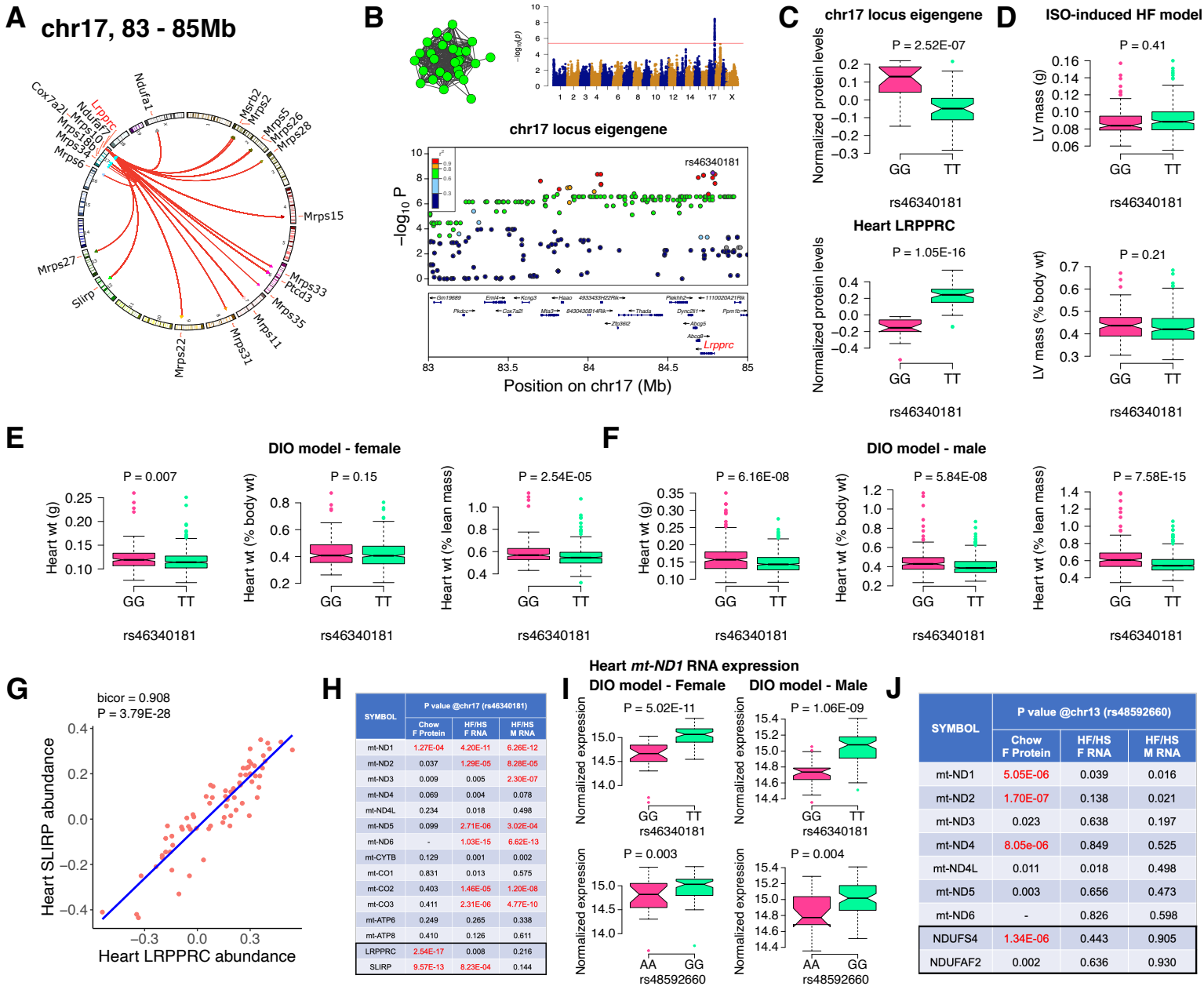

SYMBOL	P value @chr17 (rs46340181)		
	Chow F Protein	HF/HS F RNA	HF/HS M RNA
mt-ND1	1.27E-04	4.20E-11	6.26E-12
mt-ND2	0.037	1.29E-05	8.28E-05
mt-ND3	0.009	0.005	2.30E-07
mt-ND4	0.069	0.004	0.078
mt-ND4L	0.234	0.018	0.498
mt-ND5	0.099	2.71E-06	3.02E-04
mt-ND6	-	1.03E-15	6.62E-13
mt-CYTB	0.129	0.001	0.002
mt-CO1	0.831	0.013	0.575
mt-CO2	0.403	1.46E-05	1.20E-08
mt-CO3	0.411	2.31E-06	4.77E-10
mt-ATP6	0.249	0.265	0.338
mt-ATP8	0.410	0.126	0.611
LRPPRC	2.54E-17	0.008	0.216
SLIRP	9.57E-13	8.23E-04	0.144

SYMBOL	P value @chr13 (rs48592660)		
	Chow F Protein	HF/HS F RNA	HF/HS M RNA
mt-ND1	5.05E-06	0.039	0.016
mt-ND2	1.70E-07	0.138	0.021
mt-ND3	0.023	0.638	0.197
mt-ND4	8.05e-06	0.849	0.525
mt-ND4L	0.011	0.018	0.498
mt-ND5	0.003	0.656	0.473
mt-ND6	-	0.826	0.598
NDUFS4	1.34E-06	0.443	0.905
NDUFAF2	0.002	0.636	0.930

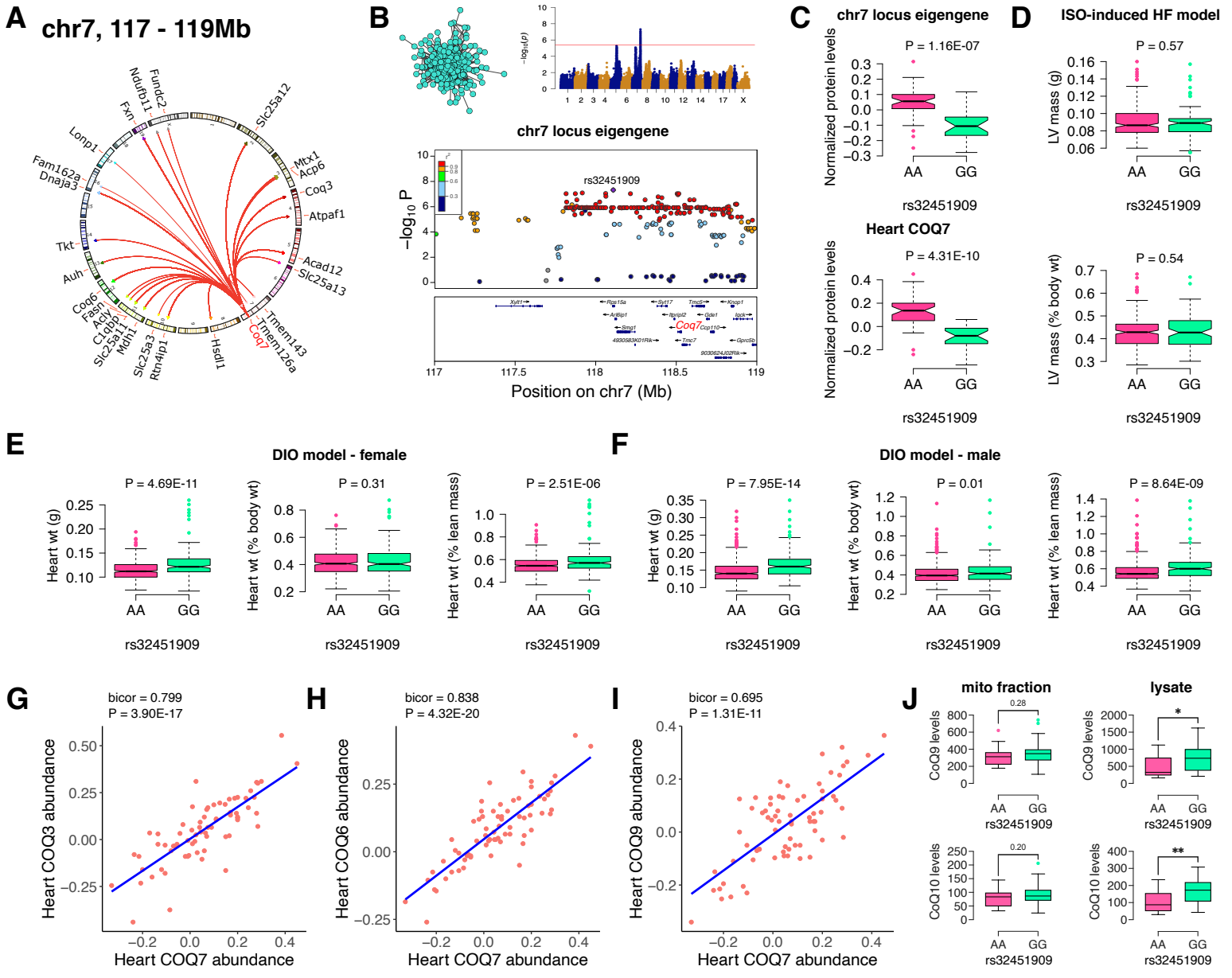
A
chr7, 117 - 119Mb
Fundc2
Ndufb11
Fxn
Slc25a12
Lonp1
Fam162a
Dnaja3
Mtx1
Acp6
Coq3
Atpaf1
Tkt
Auh
Acad12
Slc25a13
Coq6
Fasn
Acly
Cldnd1
Slc25a11
Mdh1
Slc25a3
Rtn4ip1
Hsdl1
Coq7
Tmem126a
Tmem143
B
chr7 locus eigengene
rs32451909
−log10 P
Position on chr7 (Mb)
C
chr7 locus eigengene
P = 1.16E-07
Normalized protein levels
AA
GG
rs32451909
Heart COQ7
P = 4.31E-10
D
ISO-induced HF model
P = 0.57
LV mass (g)
P = 0.54
LV mass (% body wt)
E
DIO model - female
P = 4.69E-11
Heart wt (g)
P = 0.31
Heart wt (% body wt)
P = 2.51E-06
Heart wt (% lean mass)
F
DIO model - male
P = 7.95E-14
P = 0.01
P = 8.64E-09
G
bicor = 0.799
P = 3.90E-17
Heart COQ3 abundance
Heart COQ7 abundance
H
bicor = 0.838
P = 4.32E-20
Heart COQ6 abundance
I
bicor = 0.695
P = 1.31E-11
Heart COQ9 abundance
J
mito fraction
lysate
CoQ9 levels
CoQ10 levels
0.28
0.20
*
**